ENVIRONMENTAL RESEARCH
LETTERS

LETTER • OPEN ACCESS

Using Lidar technology to assess regional air pollution and improve estimates of $PM_{2.5}$ transport in the North China Plain

To cite this article: Yan Xiang *et al* 2020 *Environ. Res. Lett.* **15** 094071

Environmental Research Letters

LETTER

Using Lidar technology to assess regional air pollution and improve estimates of $PM_{2.5}$ transport in the North China Plain

Yan Xiang[1,2,4], Lihui Lv[1,2], Wenxuan Chai[3], Tianshu Zhang[2,1], Jianguo Liu[1] and Wenqing Liu[2,1]

[1] Institutes of Physical Science and Information Technology, Anhui University, Hefei 230601, People's Republic of China
[2] Key Laboratory of Environment Optics and Technology, Anhui Institute of Optics and Fine Mechanics, Chinese Academy of Sciences, Hefei 230031, People's Republic of China
[3] Air Monitoring Department, China National Environmental Monitoring Center, Beijing 100012, People's Republic of China
[4] Author to whom any correspondence should be addressed.

E-mail: yxiang@ahu.edu.cn

OPEN ACCESS

RECEIVED
28 January 2020

REVISED
27 May 2020

ACCEPTED FOR PUBLICATION
15 June 2020

PUBLISHED
27 August 2020

Keywords: aerosols, regional transport, lidar, WRF-Chem, GSI, data assimilation

Supplementary material for this article is available online

Abstract

Air pollutants seriously impact climate change and human health. In this study, the gridpoint statistical interpolation (GSI) three-dimensional variational data assimilation system was extended from ground data to vertical profile data, which reduced the simulation error of the model in the vertical layer. The coupled GSI-Lidar-WRF-Chem system was used to improve the accuracy of fine particulate matter ($PM_{2.5}$) simulation during a wintertime heavy pollution event in the North China Plain in late November 2017. In this experiment, two vehicle-mounted Lidar instruments were utilized to make synchronous observations around the 6th Ring Road of Beijing, and five ground-based Lidars were used for long-term network observations on the North China Plain. Data assimilation was then performed using the $PM_{2.5}$ vertical profile retrieved from the seven Lidars. Compared with the model results, the correlation of assimilation increased from 0.74–0.86, and the root-mean-square error decreased by 36.6%. Meanwhile, the transport flux and transport flux intensity of the $PM_{2.5}$ were analyzed, which revealed that the $PM_{2.5}$ around the 6th Ring Road of Beijing was mainly concentrated below 1.8 km, and there were obvious double layers of particles. Particulates in the southwest were mainly input, while those in the northeast were mainly output. Both the input and output heights were around 1 km, although the input intensity was higher than the output intensity. The GSI-Lidar-WRF-Chem system has great potential for air quality simulation and forecasting.

1. Introduction

As the most populous country in the world, China is facing serious challenges from the environmental pollution associated with the rapid industrial development in recent years (Qiang *et al* 2011). Fine particulate matter ($PM_{2.5}$) is the most prominent pollutant in China, which ranks among the most polluted countries in the world (Zhang and Cao 2015, Lv *et al* 2017a). Meanwhile, $PM_{2.5}$ exerts serious impacts on sustainable urban development, the ecological environment, and human health (Carmichael *et al* 2009, Michiels *et al* 2012, Silva 2015). Studies have shown that $PM_{2.5}$ pollution contributes to more than 1 million premature deaths in China each year (Zhang *et al* 2017, Wang *et al* 2017, Ren *et al* 2017) and originates primarily from local emissions and regional transport (Subramanian *et al* 2007, Ck *et al* 2010, Udduttula 2014, Ho *et al* 2015). Therefore, providing an accurate three-dimensional distribution of $PM_{2.5}$ is particularly important for the analysis of $PM_{2.5}$ sources and for the government departments that specify emission reduction decisions (Zhang *et al* 2015, Gao *et al* 2015, Sun *et al* 2016).

Observations and air quality models are the key methods used to obtain the regional distribution characteristics of $PM_{2.5}$. Lidar can capture the vertical distribution of $PM_{2.5}$ *in situ* (Ortiz-Amezcua *et al* 2017, Osborne *et al* 2019, Foth *et al* 2019), while the regional distribution of $PM_{2.5}$ requires help from the WRF-Chem, CMAQ, and other air quality models (Campbell *et al*, 2017, Cuchiara *et al* 2017, Bran

and Srivastava 2017, Podrascanin 2019). These air quality models include large uncertainties in their $PM_{2.5}$ simulation results, however, with the errors mainly originating from emission inventory, meteorological conditions, and various model assumptions (Tsao *et al* 2012, Crippa *et al* 2016, Li *et al* 2018). Meanwhile, the development in recent years of deep learning models, machine learning, and other dependent computer models has also resulted in improved performance (Vu *et al* 2019, Smith *et al* 2019), although since these models are black boxes independent of physical relationships, the impacts of input variables cannot be analyzed. Fortunately, data assimilation (DA) is a powerful technique for combining models and observations, which can be used to correct model simulation results, greatly increase simulation accuracy, and improve precision (Maxwell *et al* 2009, Zhang *et al* 2016, Ma *et al* 2018).

In recent years, however, the assimilation of particulate matter data has mainly focused on ground observation data (Jiang *et al* 2013, Gao 2015, Gao *et al* 2017, Robichaud 2017) and satellite remote sensing data (Liu *et al* 2011, Schwartz *et al* 2012, Saide *et al* 2013, 2014, 2015), while the DA of Lidar data has rarely been examined.

In this study, two vehicle-mounted Lidars were first used to make synchronous observations along the 6th Ring Road of Beijing, and five ground-based Lidars (Chen *et al* 2016, Xiang *et al* 2019) were employed for long-term network observations on the North China Plain. Second, a model for the conversion of the extinction coefficient to aerosol mass concentration was utilized to invert the vertical $PM_{2.5}$ concentration. Third, the observed vertical $PM_{2.5}$ and the simulated results obtained using WRF-Chem were coupled to the gridpoint statistical interpolation three-dimensional variational (GSI 3DVAR) DA system (Pagowski *et al* 2014), and $PM_{2.5}$ data with high precision were obtained by correcting the measured data. Finally, the transport flux (TF) and the transport flux intensity (TFI) of the $PM_{2.5}$ in the region were analyzed. In addition, pollution transport paths were evaluated using the backward trajectory model.

2. Materials and methods

2.1. Instrumentation

The overall structure of the Mie Lidar system consists of an emitting system, receiving system, data acquisition system, control system, and GPS system (Lv *et al* 2017b). The emitting system comprises a laser and an emission optical unit. The receiving system is designed based on the principle of the Cassegrain optical telescope, which has a 1-mard receiving field of view with a vertical resolution of 7.5 m. The data acquisition and control system comprise one of the key components used to determine the data quality of the Lidar. In addition, the response speed, bandwidth, dynamic range, and signal-to-noise ratio of the measured electronic system directly determine the spatial and temporal resolutions of the Lidar system and the analytical ability of weak signals. The main technical parameters of the Lidar system are listed in table S1 (available online at stacks.iop.org/ERL/15/094071/mmedia). Additional details regarding the ground-based Lidar information can be found in Xiang *et al* (2019).

2.2. Experimental

In this study, we established two vehicle-mounted Lidars and five ground-based Lidar networks, covering the Beijing-Tianjin-Hebei region. The two vehicle-mounted Lidars performed closed observations along the 6th Ring Road of Beijing at 1:40 p.m. local time on 27 November 2017. One vehicle started north of the 6th Ring Road and traveled clockwise to the starting point, while the other vehicle started south of the 6th Ring Road. The observation route of the 6th Ring Road in Beijing is depicted by the red curve in figure 1. The 6th Ring Road in Beijing is a circular expressway with four lanes in two directions and a total length of approximately 187.6 km. The vehicle speed was set to 70 km h^{-1} in order to maximize the detection precision, detection time, and other factors. The two vehicles returned to the starting position at 4:20 p.m. on the same day. Meanwhile, the blue stars in figure 1 represent the five ground-based Lidar networks, which were used for long-term continuous observations of the Beijing-Tianjin-Hebei region. The observation data from 26–29 November 2017, were selected to analyze the pollution status of the Beijing-Tianjin-Hebei region.

2.3. Retrieval method

2.3.1. Particle extinction coefficient

The Lidar equation for the retrieved aerosol Lidar signal can be written as

$$P(z,\lambda) = \frac{KP_0(\lambda)A\Delta Z}{Z^2}\left[\beta_m(z,\lambda)+\beta_\alpha(z,\lambda)\right] \exp\left\{-2\int_{z_0}^{z}\left[\alpha_\alpha(z,\lambda)+\alpha_m(z,\lambda)\right]dz\right\} \quad (1)$$

where $P(z,\lambda)$ is the received aerosol Lidar signal at the height of z, λ is the wavelength of laser, K is the correction constant related to the Lidar system, $P_0(\lambda)$ is the power to launch a laser beam, A is the optical receiving area of the receiving telescope, and z_0 is the height of the Lidar system. $\beta_\alpha(z,\lambda)$ and $\beta_m(z,\lambda)$ are the aerosol backscatter coefficient and molecular backscatter coefficient, respectively. $\alpha_\alpha(z,\lambda)$ and $\alpha_m(z,\lambda)$ the aerosol extinction coefficient and molecular extinction coefficient, respectively.

Previous studies have shown that compared with the Collis method (Collis and Russell 1976) and

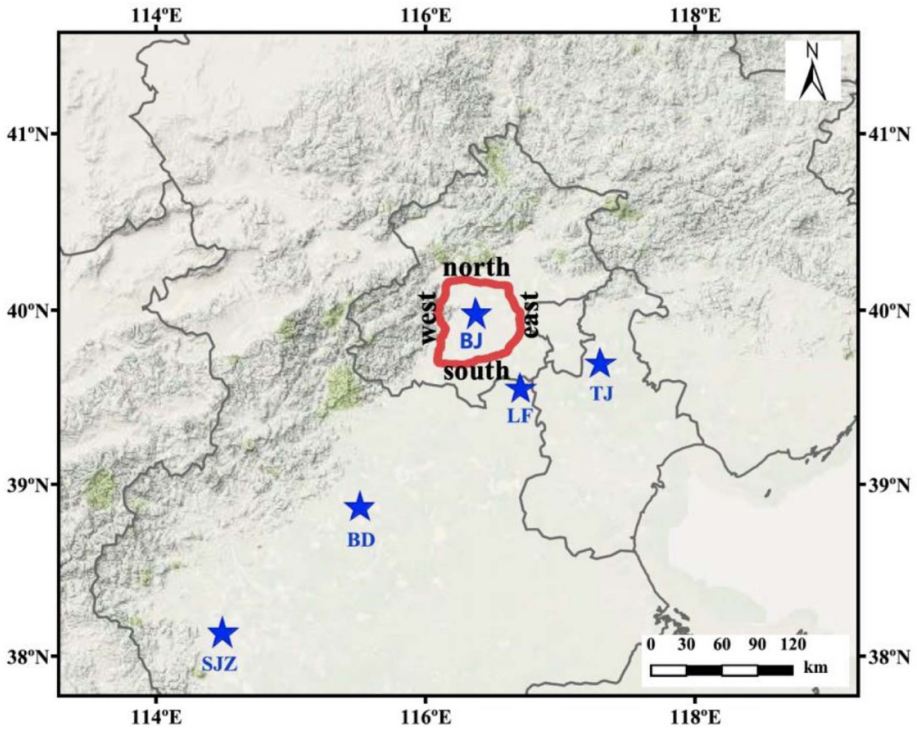

Figure 1. Locations of field observation sites. The red curve is the monitoring path of the vehicle-mounted Lidar. The blue stars represent the ground-based Lidar networks, BJ, LF, TJ, BDm and SJZ signify Beijing, Langfang, Tianjin, Baoding, and Shijiazhuang, respectively.

the Klett method (Klett 1981), the Fernald method (Fernald 1984) was the most stable, mature, and accurate inversion method. Therefore, the extinction coefficient of aerosols was retrieved using the Fernald method. The Fernald method assumes that the scattering of particles is proportional to the extinction coefficient for both aerosols and molecules. As shown in the following equations (2) and (equation (3)), where S_a is the ratio of extinction coefficient and backscatter coefficient in atmospheric aerosol (usually also referred to as the Lidar ratio), which was set as 50 Sr in this study. Moreover, S_m is the ratio of extinction coefficient and backscatter coefficient in atmospheric molecules, which was calculated as $8\pi/3$ according to the atmospheric molecular model

$$S_a = \frac{\alpha_\alpha(R_c)}{\beta_\alpha(R_c)} \tag{2}$$

$$S_m = \frac{\alpha_m(R_c)}{\beta_m(R_c)}. \tag{3}$$

Therefore, the equation (equation (1)) for the aerosol extinction coefficient can be written as:

$$\alpha_a(z) = -\frac{S_a}{S_m}\cdot\alpha_m(z) + \frac{P(z)Z^2\cdot\exp\left[2\left(\frac{S_a}{S_m}-1\right)\int_z^{z_c}\alpha_m(z\prime)\,dz\prime\right]}{\frac{P(z)Z^2}{\alpha_a(z_c)+\frac{S_a}{S_m}\alpha_m(z_c)} + 2\int_z^{z_c}P(z\prime)z\prime^2\cdot\exp\left[2\left(\frac{S_a}{S_m}-1\right)\int_z^{z_c}\alpha_m(z\prime\prime)\,dz\prime\prime\right]dz\prime} \tag{4}$$

where z_c is the reference point, which height is the minimum aerosol concentration and has a high enough signal-to-noise ratio.

2.3.2. $PM_{2.5}$ mass concentration profile.

Previous studies have shown that the extinction coefficient of aerosols is closely related to the concentration of particulate matter (Li and Han 2016, Tao *et al* 2016). Based on single-scattering theory, the formula for converting the aerosol extinction coefficient (α) profile to particle mass concentration ($PM_{2.5}$) can be expressed as follows (Tao *et al* 2016, Lv *et al* 2017b):

$$PM_{2.5} = \frac{4\rho r_{eff}\eta}{3Q_{ext}}\alpha = \delta * \alpha, \tag{5}$$

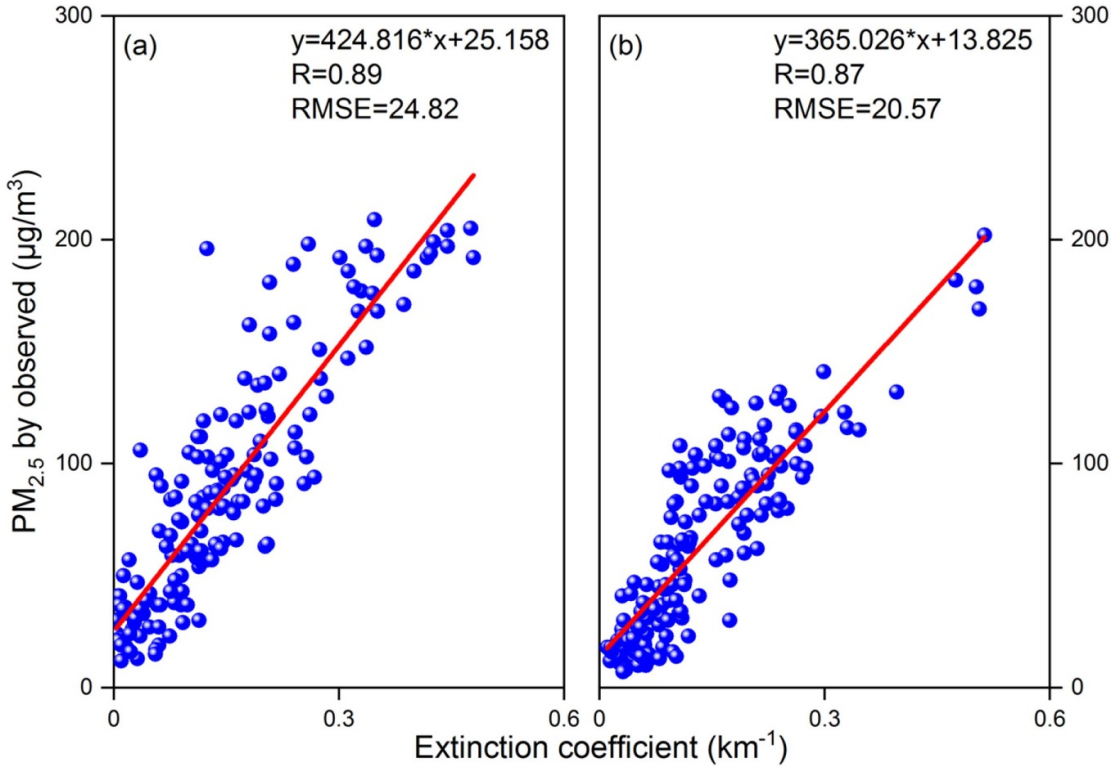

Figure 2. Linear analysis of the aerosol extinction coefficient at 0.1 km and the $PM_{2.5}$ mass concentration measured in (a) Shijiazhuang and (b) Baoding. The red line is the fitting curve between the extinction coefficient and the $PM_{2.5}$ concentration.

where $\delta = \frac{4\rho r_{eff}\eta}{3Q_{ext}}$ is the proportion coefficient determined by the aerosol size distribution, components, and optical refractive index. In addition, ρ in equation (5) represents the aerosol mass density, $r_{eff} = \frac{\int_0^\infty r^3 n(r)dr}{\int_0^\infty r^2 n(r)dr}$ depicts the effective radius of the particle, and $n(r)$ is the aerosol size distribution, Q_{ext} represents the extinction efficiency factor, and $\eta = \frac{PM_{2.5}}{PM_{total}}$ is the ratio of the $PM_{2.5}$ mass concentration to the total mass concentration.

Considering the unstable factors in the measurement (e.g. system deviation), a constant C was added to equation (5). Thus, the final formula for the $PM_{2.5}$ mass concentration in the linear model can be expressed as

$$PM_{2.5} = \delta * \alpha + C. \quad (6)$$

Therefore, in the linear fitting of the near ground extinction coefficient (α) provided by the Lidar and the ground surface $PM_{2.5}$ mass concentration observed synchronously *in situ*, the slope and intercept were obtained by the fitting corresponding to the values of δ and C in equation (6).

In order to evaluate the accuracy of the model, the data from the two most polluted observation stations (Shijiazhuang City and Baoding City) were selected. The fitting results between the extinction coefficient at 0.1 km and the measured surface $PM_{2.5}$ concentration are presented in figure 2, revealing that the correlations were 0.89 and 0.87, respectively, and the corresponding root-mean-square errors (RMSEs) were 24.82 and 20.57 $\mu g\ m^{-3}$, indicating that the model is reliable.

2.4. Model and DA system

2.4.1. Modeling of regional $PM_{2.5}$ production

The WRF-Chem chemical transport model (version 3.8.1) was used to investigate the $PM_{2.5}$ concentration. Figure S1 shows the model configuration with three nested domains with 100 × 100 (d01, 36 km), 103 × 103 (d02, 12 km), and 151 × 127 (d03, 4 km) grids, and the center was located at 36.228 N, 111.278 E. All of the domains had 101 vertical sigma layers from the ground level to the top pressure of 50 hPa. To better simulate the situation within the boundary layer, the resolution of the boundary layer was set higher, and 34 layers were set in the range of 0–2 km. The model time steps were set to 180 s and the output was released every hour. The initial and boundary meteorological conditions were derived from the 6 h National Centers for Environmental Prediction Final Analysis data with 1° × 1° spatial resolution. The anthropogenic emissions were obtained from MEIC data with 0.25° × 0.25° resolution (Zhou *et al* 2017). Terrestrial biogenic emissions were estimated using the MEGAN model (Chatani *et al* 2011). The

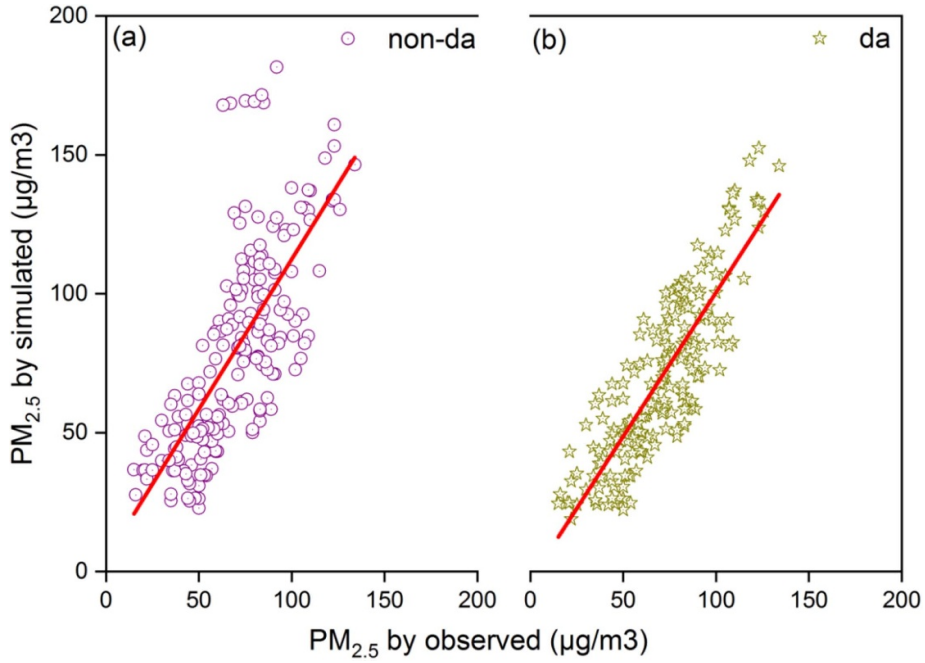

Figure 3. Comparisons of unassimilated and assimilated results of hourly $PM_{2.5}$ concentrations at multiple sites around in Beijing and its surrounding areas.

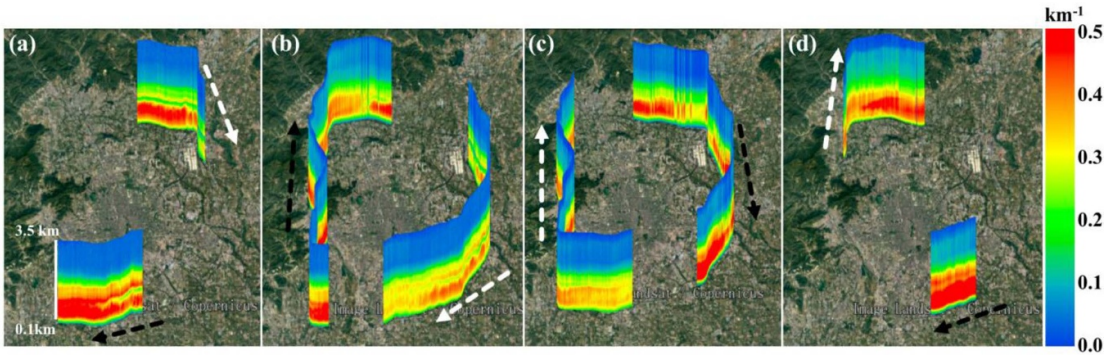

Figure 4. Spatial distribution of aerosol extinction at (a) 2:00 p.m., (b) 3:00 p.m., (c) 4:00 p.m., and (d) 5:00 p.m. on 27 November 2017.

gas-phase chemistry module CBM-Z and the aerosol module Model for Simulating Aerosol Interactions and Chemistry were used in this simulation.

2.4.2. Data assimilation system

The GSI DA system provides a 3DVAR analysis by minimizing the cost function as shown below (Gao *et al* 2017):

$$J(x) = (x - x_b)^T B^{-1} (x - x_b) + (y - H(x))^T R^{-1} (y - H(x)). \quad (7)$$

In this equation, x is the analysis vector, x_b denotes the background vector, y is an observation vector, B represents the background error covariance matrix, R represents the observation error covariance matrix, and H is the observation operator used to transform model grid point values to observed quantities, which is achieved via interpolation.

The hourly profile $PM_{2.5}$ concentrations of the two sets of Lidar data within 1 h windows were assimilated. The observation errors of the Lidar data originated from measurement errors and representative errors. The measurement error was computed using $\varepsilon_0 = 1.5 + 0.0075^*\text{obs}$ (Schwartz *et al* 2012, Jiang *et al* 2013, Gao *et al* 2017), where obs indicates the observed values. The representative error was computed using $\varepsilon_r = \gamma\sqrt{\Delta x/L}$ (Pagowski *et al* 2014), where γ is the adjustable scale factor, Δx is the model grid resolution (we selected 4 km for the domain), and L is the influencing radius (we used 60 km for the Lidar).

Figure 3 shows a comparison of the non-DA, DA, and observed values, in which the observed values of $PM_{2.5}$ were provided by the

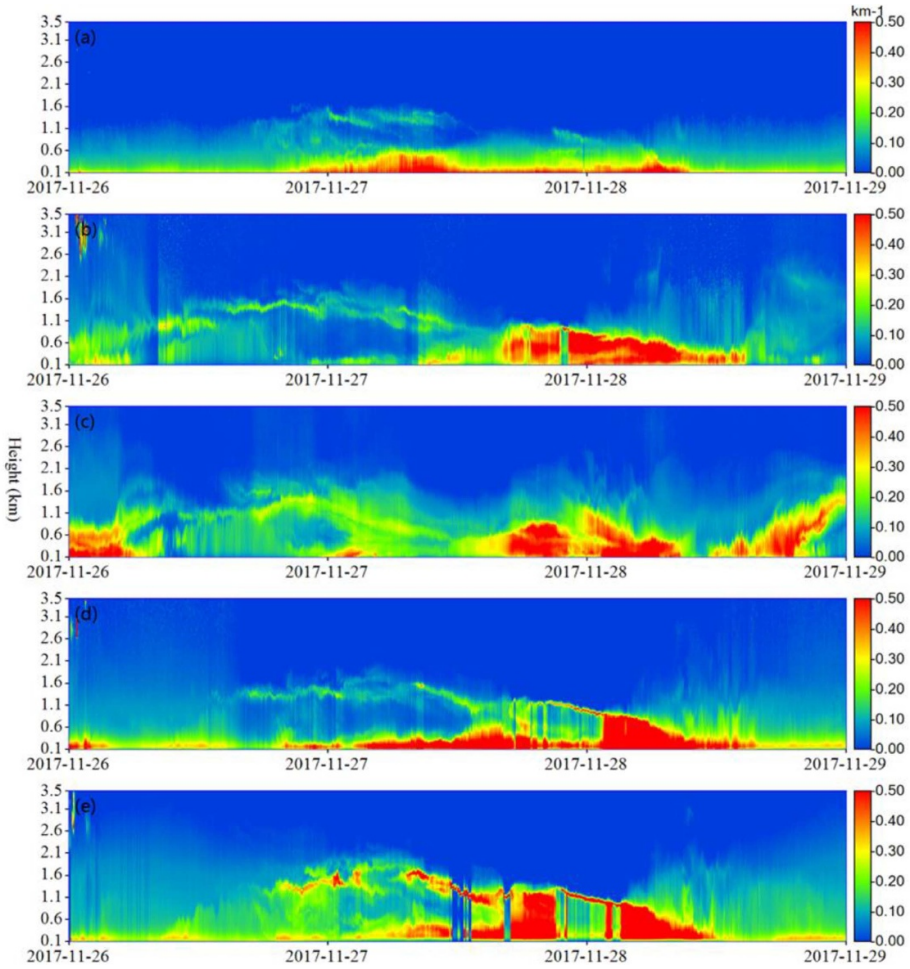

Figure 5. Continuous observation results of ground-based Lidar from 26–29 November 2017: (a) Beijing, (b) Baoding, (c) Shijiazhuang, (d) Langfang, and (e) Tianjin.

China National Environmental Monitoring Center (http://106.37.208.233:20035). These results clearly indicate that the Lidar data were a significant improvement over the simulation results. The correlation values of the non-DA and DA data were 0.74 and 0.86, respectively, representing an increase of 16.2%. Additionally, the RMSEs of the non-DA and DA data were 24.62 and 15.60 μg m^{-3}, respectively, representing a decrease of 36.6%.

2.4.3. Retrieval method for TF and TFI

Equation (8) was used to calculate the TF of the $PM_{2.5}$ based on the revised $PM_{2.5}$ concentration after assimilation and the wind field data from the simulation:

$$\text{Flux} = PM_{2.5}{}^{*}WS{}^{*}Cos\left((WD - dir){}^{*}\frac{\pi}{180}\right). \quad (8)$$

In this equation, $PM_{2.5}$ (μg m^{-3}) is the concentration of particulate matter at the current height; *WS* (m/s) and *WD* are the wind speed and wind direction at the same position, respectively; *dir* represents the angle between the current position and the direction of the transport pathway; and Flux (μg m^{-2} s^{-1}) represents the TF of the $PM_{2.5}$ at the current position. Thus, positive values of Flux signify input fluxes, while negative values signify output fluxes. The TFI of the $PM_{2.5}$ was calculated by integrating the TF of the $PM_{2.5}$.

3. Results and discussion

3.1. Meteorological conditions

Figure S2 shows the wind field distribution at 4:00 p.m. on 26, 27, and 28 November 2017, which had respective winds from the southeast, southwest, and northwest, and these wind directions at the surface were consistent with those of the upper air. On the North China Plain, the average surface wind speeds for the 3 d were 3.3, 5.0, and 7.6 m s^{-1}, respectively, while the average wind speeds 1 km above the surface were 5.1, 10.7, and 10.9 m s^{-1}, respectively. For Beijing, the average surface wind speeds on the 26th and 27th were < 2 m s^{-1}, causing pollutants to accumulate (Slater *et al* 2020). Correspondingly, the average upper air wind speeds were > 6 m s^{-1}, which was conducive to the transport of pollutants at upper levels. Meanwhile, the overall wind speeds at both the surface and upper levels in Beijing were relatively high on the 28th, which was conducive to the diffusion of pollutants by the northwest winds.

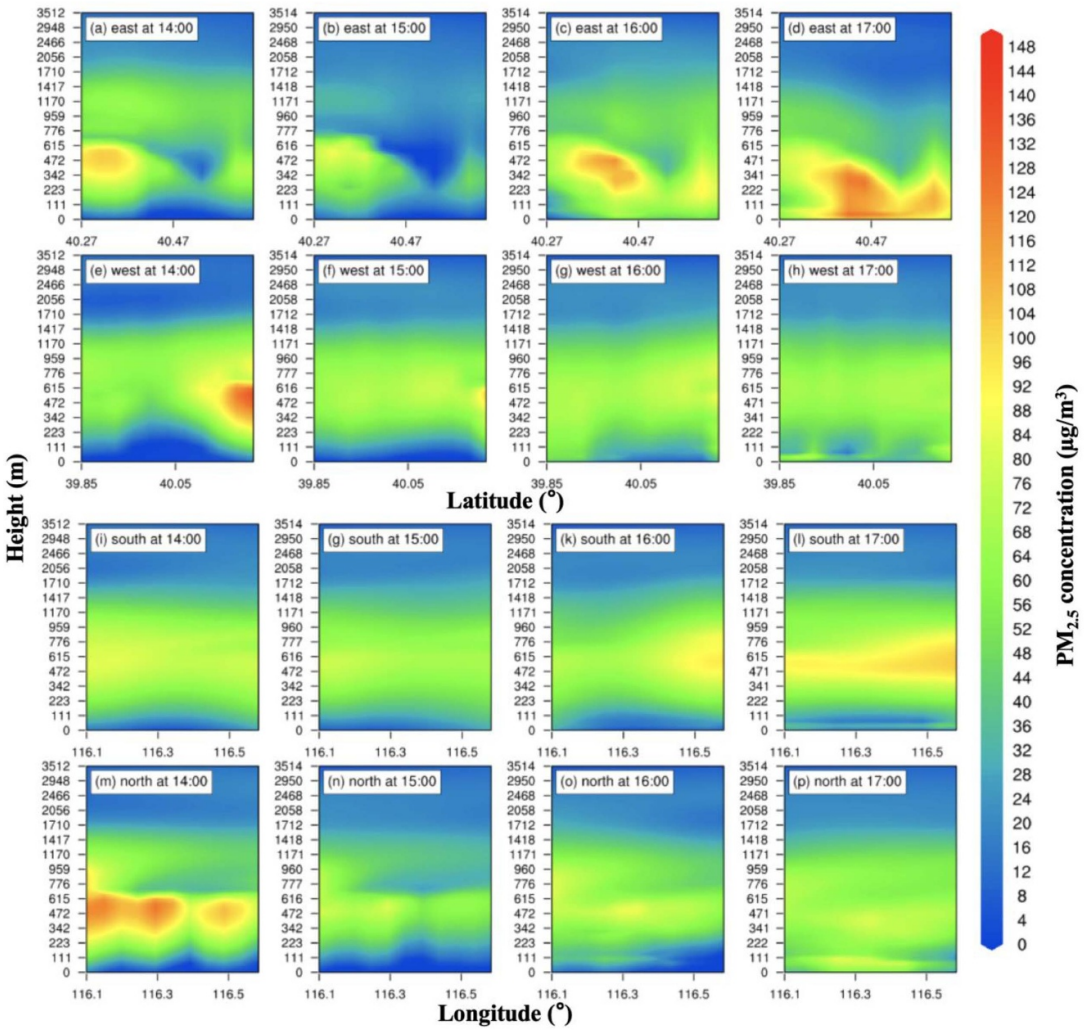

Figure 6. $PM_{2.5}$ concentration (unit: $\mu g\ m^{-3}$) along the 6th Ring Road, Beijing. The *x*-axis is (a–h) latitude and (i–p) longitude in degrees. The *y*-axis is the height in meters. The locations represented by east, west, south, and north in the upper left corner correspond to the locations labeled in figure 1.

3.2. Particle extinction coefficient

The Fernald method was used to invert the Lidar data, thereby obtaining the extinction coefficient profile (Lv *et al* 2016). As shown in figure 4, the particles were mainly concentrated below 1.8 km during the observation period, appearing in decoupled layers. Additionally, the data obtained by the two Lidar systems exhibited good consistency. The maximum extinction coefficient was 1.2 km^{-1}, which occurred at 0.8 km. The stratification of the upper-air and surface pollutants had disappeared by 5:00 p.m.

In order to further examine the paths of pollutant transport, figure 5 shows the observation results of the extinction coefficient for the five ground-based Lidars on the North China Plain from 26–29 November 2017. We found that pollutants began to accumulate in Shijiazhuang, Baoding, and other areas in the early morning of the 26th. Meanwhile, under the influence of the southwest wind, pollutants began to travel in the direction of Shijiazhuang, Baoding, and Beijing, with the transport height increasing from 0.6 km in the morning to 1.6 km at night, resulting in high concentrations of pollution in Beijing, Langfang, and other cities. The height of the pollutants began to decrease during the day on the 27th, with the pollutants reaching their peak values on the night of the 27th and in the early morning of the 28th, and the maximum extinction coefficient exceeding 1.5 km^{-1}. During the day on the 28th, under the action of northwest winds, pollutant advection began from north to south. The pollutants in Beijing, Tianjin, Langfang, and Baoding were successively reduced, while the pollutant diffusion conditions in Shijiazhuang were relatively poor due to the low wind speed.

3.3. $PM_{2.5}$ mass concentration

Figure 6 presents the spatial distribution of the $PM_{2.5}$ concentration after DA using the two sets of Lidar data. At 2:00 p.m., the $PM_{2.5}$ appeared in decoupled layers, of which the heavily polluted layer was 200–700 m. At the same time, a layer of low-concentration

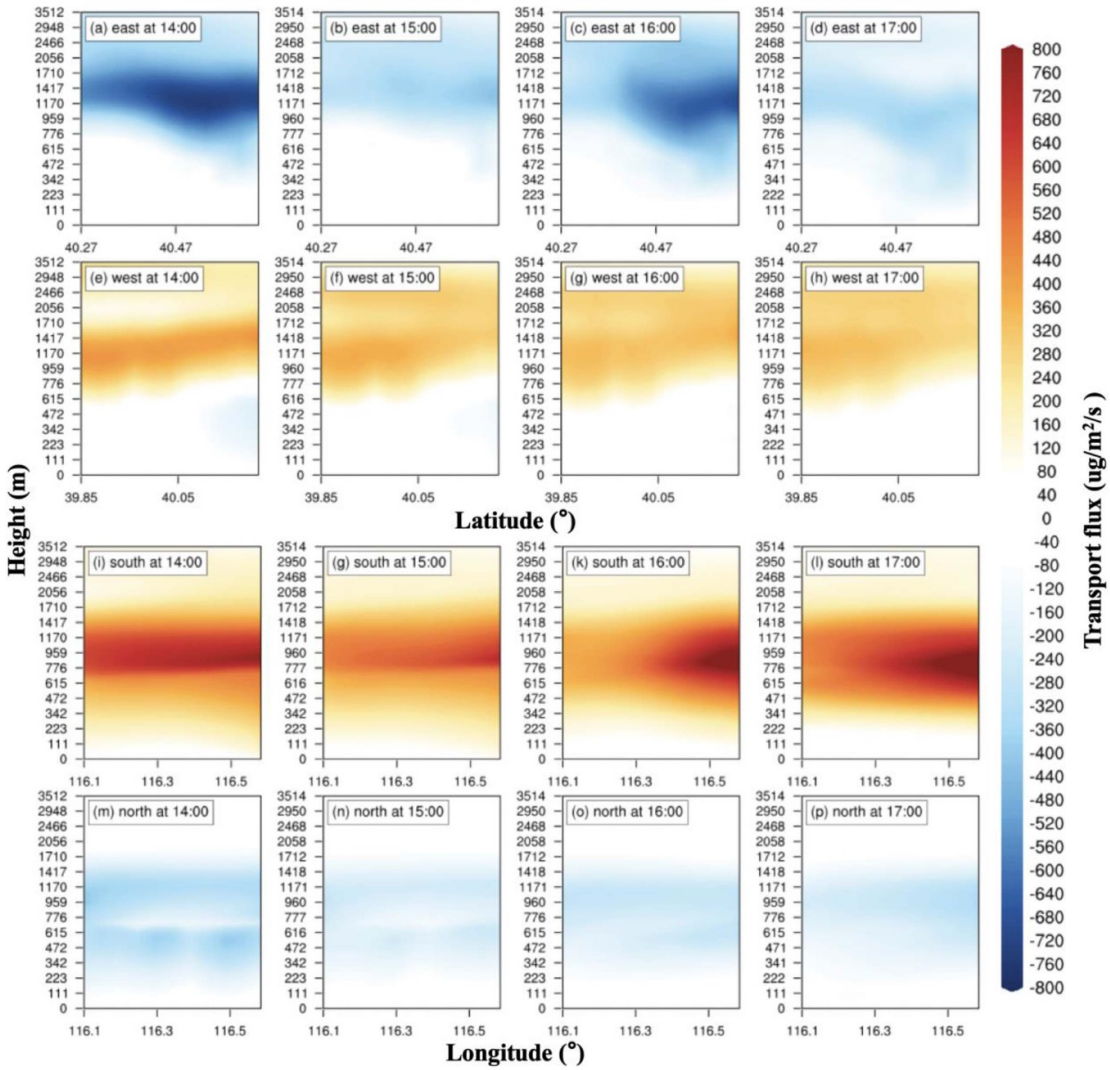

Figure 7. The same as figure 6 but for TF results (unit: μg m^{-2} s^{-1}) of $PM_{2.5}$ along the 6th Ring Road, Beijing.

pollution appeared, ranging from 700–1700 m. These findings are consistent with the Lidar observation results, confirming that the results of the Lidar assimilation system were correct. At 2:00 p.m., the $PM_{2.5}$ concentration in northwest Beijing was high, with an upper air concentration of 135 μg m^{-3}; the surface concentration, however, was only about 30 μg m^{-3}. When combined with the meteorological results from the WRF-Chem simulation, an updraft near the ground was revealed, which caused the pollutants to spread out into the ambient atmosphere. Hence, the concentration of pollutants near the ground was low. Under the influence of the southwest wind flow, pollutants ahead of the Taihang Mountains were transported to Beijing, causing the $PM_{2.5}$ concentration in southwest Beijing to reach its maximum at 5:00 p.m. At the same time, the pollutant height decreased, causing the $PM_{2.5}$ concentration at the surface to reach 126 μg m^{-3}. Meanwhile, in order to further estimate the possible sources and transport pathways of the aerosols, the backward and forward trajectory analyses from the HYSPLIT model are presented in figure S3.

3.4. TF of $PM_{2.5}$ and TFI of $PM_{2.5}$

Figure 7 shows the TF results of $PM_{2.5}$ along the 6th Ring Road in Beijing. A positive TF indicates that $PM_{2.5}$ was transported to Beijing; otherwise, the pollutants were exported from Beijing. Both the southern portion and the western portion of the 6th Ring Road primarily received $PM_{2.5}$ during the observation period, with the transmission occurring at 1 km. At the same time, the transmission intensity along the southern part of 6th Ring Road was higher than that along the western part of 6th Ring Road. In the northeast region of Beijing, $PM_{2.5}$ was mainly transmitted to other cities, and the transmission height was similar to that of $PM_{2.5}$ transported to Beijing in the southwest region, although the output intensity was significantly lower than the input intensity. The maximum $PM_{2.5}$ transmission values of 931 and − 701 μg m^{-2} s^{-1} in the southern

and eastern parts of the 6th Ring Road, respectively, both occurred at 4:00 p.m. Moreover, figure S4 shows the TFI results of $PM_{2.5}$ along the 6th Ring Road in Beijing. The TFI values of $PM_{2.5}$ in the eastern, southern, western, and northern parts were −1133, 847, 1060, and −457 $\mu g\ km^{-1}\ s^{-1}$, respectively, indicating that pollutants were transported from the southwest to Beijing and diffused from Beijing to the northeast.

4. Conclusion

Accurately quantifying the distribution of particulate matter in the atmosphere is the key requirement for the prediction of air quality and the estimation of atmospheric environmental capacity. In this study, the $PM_{2.5}$ data from the inversion of seven Lidars (two vehicle-mounted and five ground-based) along with simulated $PM_{2.5}$ data from the WRF-Chem were coupled to a GSI 3DVAR assimilation system. The $PM_{2.5}$ field was obtained after the observation data were corrected. When compared with the unassimilated results, the correlation of the DA results based on the Lidar data increased by 16.2%, while the RMSE decreased by 36.6%. Moreover, an analysis of the TF and TFI of the $PM_{2.5}$ revealed that the $PM_{2.5}$ along the 6th Ring Road of Beijing was mainly concentrated below 1.8 km, and there were obvious decoupled layers of particles. Particulates in the southwest were mainly input, while those in the northeast were mainly output. Both the input and output heights were around 1 km, although the input intensity was higher than the output intensity.

In addition, the discovery of the aerosol vertical characteristics on the North China Plain has numerous potential applications. Obviously, this dataset can be used to further verify and improve the representation of aerosols in air quality models and satellite remote sensing. In addition, the determination of the aerosol transport characteristics at different heights can provide evidence to explain the cross-border transport mechanism of pollutants. Moreover, the results of the data of this study can also provide technical support and services, which can be utilized by environmental management departments to evaluate the efficiency of pollution control, predict the impacts of air pollution on environmental health, and effectively carry out environmental management and pollution control.

Acknowledgments

This work was supported by the Natural Science Foundation of Anhui Province, China (1908085QD160, 1908085QD170), the National Research Program for Key Issues in Air Pollution Control (DQGG0102), the National Natural Science Foundation of China (41941011), the National Key Project of MOST (2017YFC0213002, 2018YFC0213101, 2016YFC0200401), and the Doctoral Scientific Research Foundation of Anhui University (Y040418190).

Data availability statement

The data that support the findings of this study are available from the authors upon request. The FNL data are available from the following website (https://rda.ucar.edu/datasets/ds083.2/). The data in this study were analyzed using the NCAR Command Language (http://www.ncl.ucar.edu/). The authors are grateful to the China National Environmental Monitoring Center for providing monitoring data for the $PM_{2.5}$ (http://106.37.208.233:20 035). The authors gratefully acknowledge the NOAA Air Resources Laboratory (ARL) for providing the HYSPLIT transport and dispersion model (https://ready.arl.noaa.gov/HYSPLIT_traj.php) used in this research.

ORCID iDs

Yan Xiang https://orcid.org/0000-0003-3544-9134
Jianguo Liu https://orcid.org/0000-0002-7051-4272

References

Bran S H and Srivastava R 2017 Investigation of PM2.5 mass concentration over India using a regional climate model *Environ. Pollut.* **224** 484–93

Campbell P, Yang Z, Kai W, Leung R, Fan J, Bo Z, Qiang Z and He K 2017 Evaluation of a multi-scale WRF-CAM5 simulation during the 2010 East Asian summer monsoon *Atmos. Environ.* **169** 204–17

Carmichael G R, Adhikary B, Kulkarni S, D'allura A, Tang Y, Streets D, Zhang Q, Bond T C, Ramanathan V and Jamroensan A 2009 Asian aerosols: current and year 2030 distributions and implications to human health and regional climate change *Environ. Sci. Technol.* **43** 5811–7

Chatani S, Morikawa T, Nakatsuka S, Matsunaga S and Minoura H 2011 Development of a framework for a high-resolution, three-dimensional regional air quality simulation and its application to predicting future air quality over Japan *Atmos. Environ.* **45** 1383–93

Chen Z Y, Liu W Q, Liu J G, Zhang T S and Dong Y S 2016 Using Lidar, in-situ measurements and trajectory analysis to observe air pollution in Beijing, 2014 *27th Int. Laser Radar Conf.* 119 24008

Chang S-C, Chou C C-K, Chan C-C and Lee C-T 2010 Temporal characteristics from continuous measurements of PM 2.5 and speciation at the Taipei aerosol supersite from 2002 to 2008 *Atmos. Environ.* **44** 1088–96

Collis R T H and Andrussell P B 1976 Lidar measurement of particles and gases by elastic backscattering and differential absorption *Laser Monitoring of the Atmosphere* ed E D Hinkley vol 14 (Berlin: Springer) pp 71–151

Crippa P, Sullivan R C, Thota A and Pryor S C 2016 Evaluating the skill of high-resolution WRF-Chem simulations in describing drivers of aerosol direct climate forcing on the regional scale *Atmos. Chem. Phys.* **16** 397–416

Cuchiara G C, Rappenglück B, Rubio M A, Lissi E, Gramsch E and Garreaud R D 2017 Modeling study of biomass burning plumes and their impact on urban air quality; a case study of Santiago de Chile *Atmos. Environ.* **166** 79–91

Fernald F G 1984 Analysis of atmospheric Lidar observations: some comments *Appl. Opt.* **23** 652–3

Foth A, Kanitz T, Engelmann R, Baars H, Radenz M, Seifert P, Barja B, Fromm M, Kalesse H and Ansmann A 2019 Vertical aerosol distribution in the southern hemispheric midlatitudes as observed with Lidar in Punta Arenas, Chile (53.2 degrees S and 70.9 degrees W), during ALPACA *Atmos. Chem. Phys.* **19** 6217–33

Gao M 2015 Improving understanding of haze pollution in the North China Plain via atmospheric modeling and data assimilation *PhD Thesis*, University of Iowa

Gao M, Saide P E, Xin J Y, Wang Y S, Liu Z R, Wang Y X, Wang Z F, Pagowski M, Guttikunda S K and Carmichael G R 2017 Estimates of health impacts and radiative forcing in winter haze in Eastern China through constraints of surface PM2.5 predictions *Environ. Sci. Technol.* **51** 2178–85

Gao X L, Hai Y X, Jie Q Z and Fan T J 2015 Investment strategy of emission-reduction technology in a supply chain *Sustainability* **7** 10684–708

Ho K F, Huang R J, Kawamura K, Tachibana E, Lee S C, Ho S S H, Zhu T and Tian L 2015 Dicarboxylic acids, ketocarboxylic acids, α-dicarbonyls, fatty acids and benzoic acid in PM2.5 aerosol collected during CAREBeijing-2007: an effect of traffic restriction on air quality *Atmos. Chem. Phys.* **15** 14855–87

Jiang Z Q, Liu Z Q, Wang T J, Schwartz C S, Lin H C and Jiang F 2013 Probing into the impact of 3DVAR assimilation of surface PM10 observations over China using process analysis *J. Geophys. Res. Atmos.* **118** 6738–49

Klett J D 1981 Stable analytical inversion solution for processing Lidar returns *Appl. Opt.* **20** 211–20

Li H, Duan F, Ma Y, He K, Zhu L, Ma T, Ye S, Yang S, Huang T and Kimoto T 2018 Haze pollution in winter and summer in Zibo, a heavily industrialized city neighboring the Jin-Jin-Ji area of China: source, formation, and implications *Atmos. Chem. Phys. Discuss.* **2018** 1–40

Li J W and Han Z W 2016 Aerosol vertical distribution over east China from RIEMS-chem simulation in comparison with CALIPSO measurements *Atmos. Environ.* **143** 177–89

Liu Z Q, Liu Q H, Lin H C, Schwartz C S, Lee Y H and Wang T J 2011 Three-dimensional variational assimilation of MODIS aerosol optical depth: implementation and application to a dust storm over East Asia *J. Geophys. Res. Atmos.* **116**

Lv B, Hu Y, Chang H H, Russell A G, Cai J, Bing X and Bai Y 2017a Daily estimation of ground-level PM 2.5 concentrations at 4 km resolution over Beijing-Tianjin-Hebei by fusing MODIS AOD and ground observations *Sci. Total Environ.* **580** 235–44

Lv L H, Liu W Q, Fan G Q, Zhang T S, Dong Y S, Chen Z Y, Liu Y, Huang H Y and Zhou Y 2016 Application of mobile vehicle Lidar for urban air pollution monitoring *Chin. Opt. Lett.* **14** 060101–6

Lv L H *et al* 2017b Observations of particle extinction, PM2.5 mass concentration profile and flux in north China based on mobile Lidar technique *Atmos. Environ.* **164** 360–9

Ma C Q, Wang T J, Zang Z L and Li Z J 2018 Comparisons of three-dimensional variational data assimilation and model output statistics in improving atmospheric chemistry forecasts *Adv. Atmos. Sci.* **35** 813–25

Maxwell D H, Jackson B M and Mcgregor J 2009 Using data assimilation innovations to improve model output accuracy for the highly regulated Lake Taupo catchment, New Zealand *Am. Geophysical Union* H43I-07

Michiels H, Mayeres I, Panis L I, Nocker L D, Deutsch F and Lefebvre W 2012 PM 2.5 and NO x from traffic: human health impacts, external costs and policy implications from the Belgian perspective *Transp. Res. D* **17** 569–77

Ortiz-Amezcua P *et al* 2017 Microphysical characterization of long-range transported biomass burning particles from North America at three EARLINET stations *Atmos. Chem. Phys.* **17** 5931–46

Osborne M, Malavelle F F, Adam M, Buxmann J, Sugier J, Marenco F and Haywood J 2019 Saharan dust and biomass burning aerosols during ex-hurricane Ophelia: observations from the new UK Lidar and sun-photometer network *Atmos. Chem. Phys.* **19** 3557–78

Pagowski M, Liu Z, Grell G A, Hu M, Lin H C and Schwartz C S 2014 Implementation of aerosol assimilation in gridpoint statistical interpolation (v. 3.2) and WRF-Chem (v. 3.4.1) *Geosci. Model Dev.* **7** 1621–7

Podrascanin Z 2019 Setting-up a real-time air quality forecasting system for Serbia: a WRF-chem feasibility study with different horizontal resolutions and emission inventories *Environ. Sci. Pollut. Res.* **26** 17066–79

Qiang W, Zhou W and Liang Z 2011 China's environment: challenges and solutions *Environ. Earth Sci.* **64** 1503–4

Ren M, Fang X, Li M, Sun S, Pei L, Xu Q, Ye X and Cao Y 2017 Concentration-response relationship between PM2.5 and daily respiratory deaths in china: a systematic review and metaregression analysis of time-series studies *Biomed. Res. Int.* **2017** 5806185

Robichaud A 2017 Surface data assimilation of chemical compounds over North America and its impact on air quality and air quality health index (AQHI) forecasts *Air Qual. Atmos. Health* **10** 955–70

Saide P E, Carmichael G R, Liu Z, Schwartz C S, Lin H C, Da Silva A M and Hyer E 2013 Aerosol optical depth assimilation for a size-resolved sectional model: impacts of observationally constrained, multi-wavelength and fine mode retrievals on regional scale analyses and forecasts *Atmos. Chem. Phys.* **13** 10425–44

Saide P E, Kim J, Song C H, Choi M, Cheng Y F and Carmichael G R 2014 Assimilation of next generation geostationary aerosol optical depth retrievals to improve air quality simulations *Geophys. Res. Lett.* **41** 9188–96

Saide P E, Spak S N, Pierce R B, Otkin J A, Schaack T K, Heidinger A K, Da Silva A M, Kacenelenbogen M, Redemann J and Carmichael G R 2015 Central American biomass burning smoke can increase tornado severity in the US *Geophys. Res. Lett.* **42** 956–65

Schwartz C S, Liu Z Q, Lin H C and Mckeen S A 2012 Simultaneous three-dimensional variational assimilation of surface fine particulate matter and MODIS aerosol optical depth *J. Geophys. Res. Atmos.* **117** D13202

Silva R A 2015 Climate change, air quality and human health: quantifying the global mortality impacts of present and future ozone and pm2.5 ambient air pollution *PhD Thesis* University of North Carolina at Chapel Hill Graduate School

Slater J, Tonttila J, Mcfiggans G, Romakkaniemi S, Kühn T and Coe H 2020 Using a coupled LES-aerosol radiation model to investigate urban haze: sensitivity to aerosol loading and meteorological conditions *Atmos. Chem. Phys. Discuss.* **2020** 1–23

Smith K R, Edwards P M, Ivatt P D, Lee J D, Squires F, Dai C, Peltier R E, Evans M J, Sun Y and Lewis A C 2019 An improved low-power measurement of ambient NO_2 and O_3 combining electrochemical sensor clusters and machine learning *Atmos. Meas. Tech.* **12** 1325–36

Subramanian R, Donahue N M, Bernardo-Bricker A, Rogge W F and Robinson A L 2007 Insights into the primary–secondary and regional–local contributions to organic aerosol and PM2.5 mass in Pittsburgh, Pennsylvania *Atmos. Environ.* **41** 7414–33

Sun Y, Dong M and Qian Z 2016 Research on emission reduction decisions in multi-echelon supply chain with low-carbon policy considered *Int. Conf. on Logistics* pp 1–6

Tao Z M, Wang Z Z, Yang S J, Shan H H, Ma X M, Zhang H, Zhao S G, Liu D, Xie C B and Wang Y J 2016 Profiling the PM2.5 mass concentration vertical distribution in the boundary layer *Atmos. Meas. Tech.* **9** 1369–76

Tsao C, Campbell J E, Menacarrasco M, Spak S N, Carmichael G R and Chen Y 2012 Increased estimates of air-pollution emissions from Brazilian sugar-cane ethanol *Nat. Clim. Change* **2** 53–57

Udduttula A 2014 Contributions of local and regional sources to fine PM in the megacity of Paris *Atmos. Chem. Phys.* **14** 25769–99

Vu T V, Shi Z, Cheng J, Zhang Q, He K, Wang S and Harrison R M 2019 Assessing the impact of clean air action on air quality trends in Beijing using a machine learning technique *Atmos. Chem. Phys.* **19** 11303–14

Wang H, Zhang Y, Zhao H, Lu X, Zhang Y, Zhu W, Nielsen C P, Li X, Zhang Q and Bi J 2017 Trade-driven relocation of air pollution and health impacts in China *Nat. Commun.* **8** 738

Xiang Y, Zhang T S, Liu J G, Lv L H, Dong Y S and Chen Z Y 2019 Atmosphere boundary layer height and its effect on air pollutants in Beijing during winter heavy pollution *Atmos. Res.* **215** 305–16

Zhang Q *et al* 2017 Transboundary health impacts of transported global air pollution and international trade. *Nature* **543** 705

Zhang T L, Sun R, Peng C H, Zhou G Y, Wang C L, Zhu Q A and Yang Y Z 2016 Integrating a model with remote sensing observations by a data assimilation approach to improve the model simulation accuracy of carbon flux and evapotranspiration at two flux sites *Sci. China Earth Sci.* **59** 337–48

Zhang Y J, Wang A D and Tan W 2015 The impact of China's carbon allowance allocation rules on the product prices and emission reduction behaviors of ETS-covered enterprises *Energy Policy* **86** 176–85

Zhang Y L and Cao F 2015 Fine particulate matter (PM2.5) in China at a city level *Sci. Rep.* **5** 14884

Zhou Y D, Zhao Y, Mao P, Zhang Q, Zhang J, Qiu L P and Yang Y 2017 Development of a high-resolution emission inventory and its evaluation and application through air quality modeling for Jiangsu Province, China *Atmos. Chem. Phys.* **17** 211–33